CHEMISTRY
A EUROPEAN JOURNAL

DOI: 10.1002/chem.200903269

Elucidation of Metal-Ion Accumulation Induced by Hydrogen Bonds on Protein Surfaces by Using Porous Lysozyme Crystals Containing Rh^{III} Ions as the Model Surfaces

Takafumi Ueno,*[a, b] Satoshi Abe,[a] Tomomi Koshiyama,[a] Takahiro Ohki,[c] Tatsuo Hikage,[d] and Yoshihito Watanabe[c]

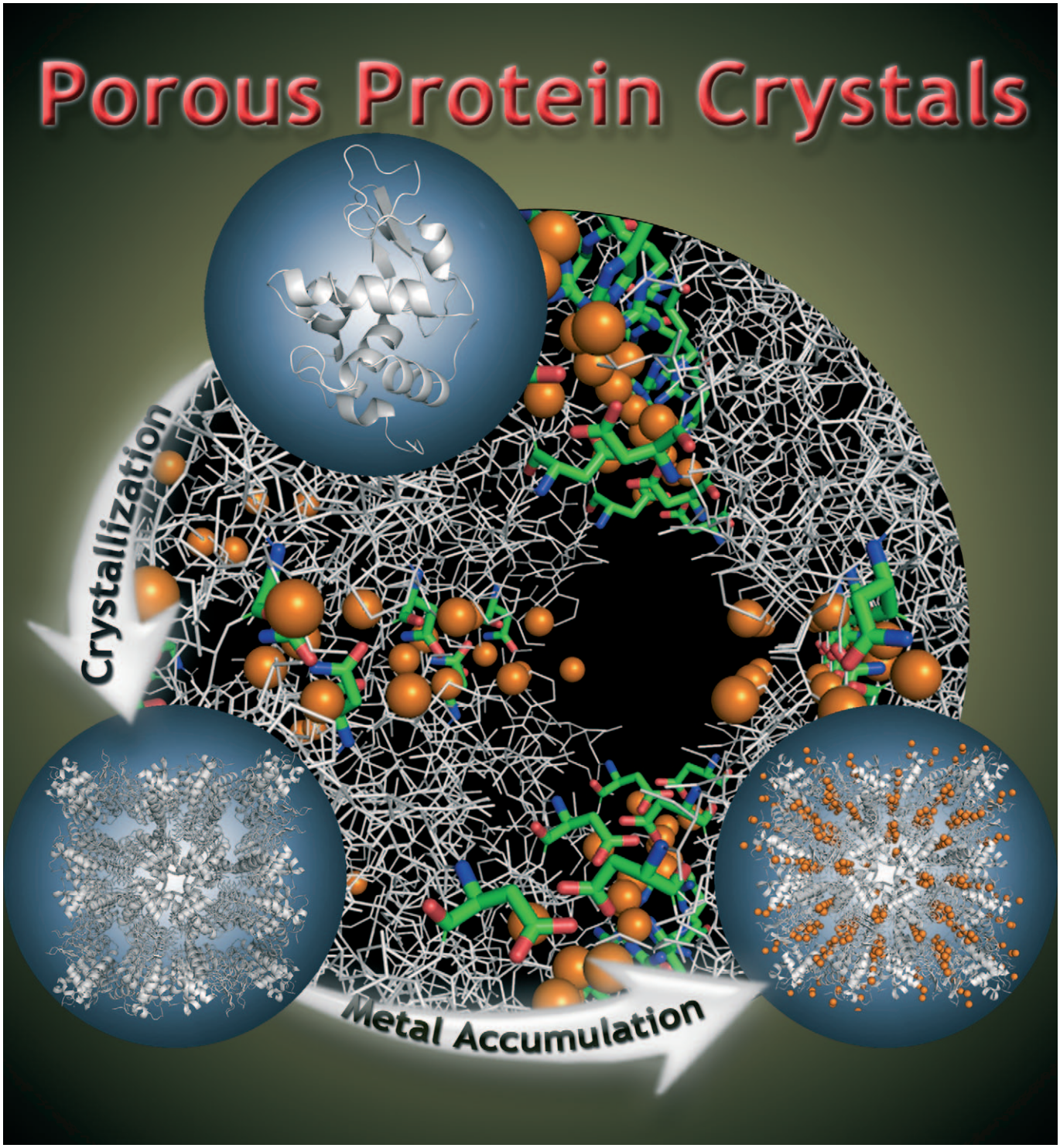

Abstract: Metal-ion accumulation on protein surfaces is a crucial step in the initiation of small-metal clusters and the formation of inorganic materials in nature. This event is expected to control the nucleation, growth, and position of the materials. There remain many unknowns, as to how proteins affect the initial process at the atomic level, although multistep assembly processes of the materials formation by both native and model systems have been clarified at the macroscopic level. Herein the cooperative effects of amino acids and hydrogen bonds promoting metal accumulation reactions are clarified by using porous hen egg white lysozyme (HEWL) crystals containing Rh^{III} ions, as model protein surfaces for the reactions. The experimental results reveal noteworthy implications for initiation of metal accumulation, which involve highly cooperative dynamics of amino acids and hydrogen bonds: i) Disruption of hydrogen bonds can induce conformational changes of amino-acid residues to capture Rh^{III} ions. ii) Water molecules pre-organized by hydrogen bonds can stabilize Rh^{III} coordination as aqua ligands. iii) Water molecules participating in hydrogen bonds with amino-acid residues can be replaced by Rh^{III} ions to form polynuclear structures with the residues. iv) Rh^{III} aqua complexes are retained on amino-acid residues through stabilizing hydrogen bonds even at low pH ($\approx$2). These metal–protein interactions including hydrogen bonds may promote native metal accumulation reactions and also may be useful in the preparation of new inorganic materials that incorporate proteins.

Keywords: bioinorganic chemistry · hydrogen bonds · protein structure · rhodium · self-assembly

Introduction

Accumulation of metal ions on proteins represents not only a natural process for creation of bioinorganic materials in nature, but is also an important strategy for use in the design of advanced inorganic materials.[1–5] Synthesis of inorganic compounds by using proteins or peptides is now attracting attention in the fast-growing field of nanomaterials science.[6–12] It is commonly known that proteins and peptides play very important roles in providing materials with various characteristics. The accumulation of metal ions on protein surfaces is, therefore, a crucial step in the preorganization of metal ions to initiate small-metal clusters and the formation of inorganic materials because this event is expected to control the nucleation, growth and position of inorganic materials.[13–19] There remain many unknowns as to how proteins affect the initial process at the atomic level. In particular, cooperative effects involved in the metal accumulation process are thought to include the dynamic behavior of amino acid side chains and hydrogen bonds, although the multistep assembly processes of biomineral formations of both native and model systems have been clarified at the macroscopic scale.[2,13,17–19]

The coordination structures of metal ions accumulated in protein cages have been investigated by X-ray crystal structural analysis of metal storage proteins.,[15,16,20–28] A Fe_3O_4 cluster is observed in the cage of Dps-like ferritin protein (DpsA) when the crystal of apo-DpsA is soaked in a cryo-buffer containing $FeCl_2$.[15] Structures of small Fe- and Hf-oxo-clusters in ferric binding protein (Fbp) indicate that a flexible binding motif can play a major role in metal accumulation to control the geometric processes.[16,29] Many crystal structures of ferritins (Frs), which include various metal ions have been reported with the aim of elucidating the metal accumulation process that occurs within the cage.[20–24] We have reported on the accumulation process of Pd^{II} ions on the interior surface of apo-ferritin (apo-Fr) by investigating a series of X-ray crystal structures of apo-Fr that contain different amounts of Pd^{II} ions. The results indicate that the number of Pd^{II} ions accumulated by apo-Fr increases when different coordination structures are adopted at the specific binding sites on the interior surface of apo-Fr.[23] However, there is only limited information about the cooperative roles of hydrogen bonds and amino-acid residues in the accumulation reactions, because the crystal structure with a high content of Pd^{II} ions was obtained at low resolution.[23,30] If we can construct appropriate metal ion/protein surface models, we expect to gain an in-depth understanding of the accumulation mechanism.

Protein crystals are expected to serve as model protein surfaces in investigations aimed at the elucidation of the mechanism of metal-ion accumulations by single-crystal X-ray structural analysis. Protein crystals have been utilized as nano-sized porous materials in applications such as separations, biocatalysis, and drug delivery because they can form various porous spaces ranging in size from 15–100 Å.[31,32] The pore size and morphologies of protein crystals are dependent on the nature and crystallization conditions of the

[a] Prof. Dr. T. Ueno, Dr. S. Abe, Dr. T. Koshiyama
Institute for Integrated Cell-Material Sciences (iCeMS)
Kyoto University
Katsura, Nishikyo-ku, Kyoto 615-8510, (Japan)
Fax: (+81) 75-383-2812
E-mail: taka@sbchem.kyoto-u.ac.jp

[b] Prof. Dr. T. Ueno
PRESTO (Japan) Science and Technology Agency (JST)
Honcho, Kawaguchi, Saitama 332-0012 (Japan)

[c] T. Ohki, Prof. Dr. Y. Watanabe
Graduate School of Science, Nagoya University
Chikusa-ku, Nagoya464-8602 (Japan)

[d] T. Hikage
High Intensity X-ray Diffraction Laboratory
Nagoya University, Chikusa-ku, Nagoya464-8602 (Japan)

Supporting information for this article is available on the WWW under http://dx.doi.org/10.1002/chem.200903269.

proteins. Functional groups of amino acid side chains, such as imidazole, thiol, amine, carboxylic acid, and phenol, are regularly exposed to internal surfaces of the crystal pores. Thus, ions and organic molecules are able to interact with the pore surfaces. Experimental and theoretical studies on the diffusion of ions and fluorescent molecules into protein crystal pores have been recently reported.[33,34] It is expected that porous protein crystals (PPCs) have the potential to provide a means for observing interactions between amino acids and various metal ions at a higher resolution than the resolution possible for crystals of apo-Fr. This is possible because more flexibility is achievable with respect to reaction conditions for PPCs (including pH, and the identity and quantity of metal ions) relative to the more restrictive conditions required for working with crystals of apo-Fr containing metal ions.[23]

We demonstrate a snapshot analysis of protein-mediated metal accumulation processes by using porous hen egg white lysozyme (HEWL) crystals that contain different amounts of Rh^{III} ions to elucidate the metal accumulation mechanism, as a preorganization of metal ions for biomineralization reactions at the atomic level. HEWL, a small hydrolytic enzyme, forms a tetragonal crystal (space group $P4_32_12$) with different types of pores, as shown in Figure 1a.[33] It has been reported that HEWL can serve as a biotemplate for preparation of inorganic materials in solution.[35–37] Moreover, the crystal has been known to capture and deposit metal complexes and metal ions when subjected to co-crystallization or soaking techniques, because the pore surfaces include coordinating amino acid residues, such as histidine, lysine, aspartate, and glutamate.[38–44] Although such coordination structures have been reported in detail, there are no reports of the dynamic behavior of amino acid residues bound to metal ions during the process of accumulation of metal ions. We have chosen the Rh^{III} ion for our experiments because; i) the metal ions are able to form several polynuclear structures under the HEWL crystallization conditions (<pH4.5), and ii) the kinetic inertness of the Rh^{III} ion enables high resolution structural determination using by single-crystal X-ray structural analysis (Figure 1b).[45] Our model system, which takes advantage of the favorable properties of PPCs of HEWL, provides direct structural evidence for the cooperative contributions of conformational changes of amino acid residues and hydrogen bonds in the metal accumulation on protein surfaces.

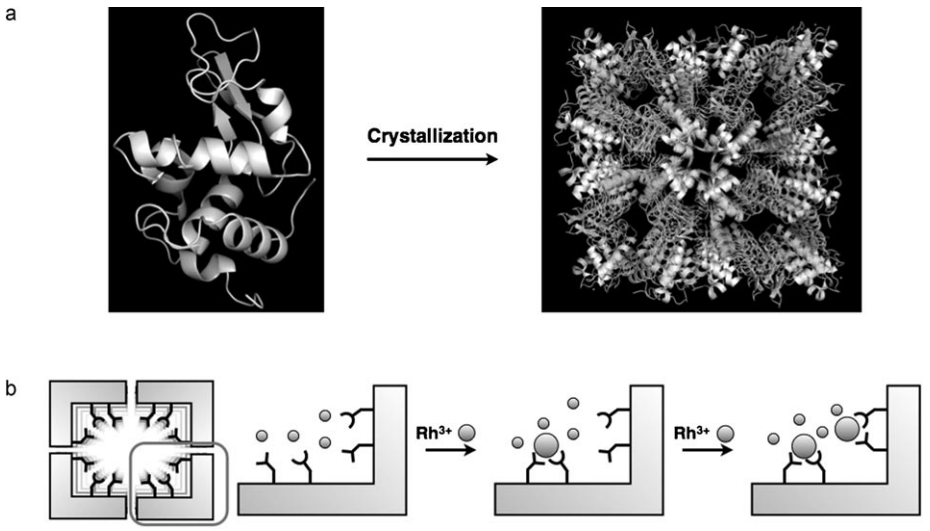

Figure 1. a) Crystal lattice structure of tetragonal HEWL crystal. b) Schematic drawings of the deposition of Rh^{III} ions in the pore of porous HEWL crystals.

Results and Discussion

Preparation and X-ray structural analysis of HEWL crystals with different amounts of Rh^{III} ions: Tetragonal HEWL crystals were prepared according to a previously reported procedure.[46] To prepare the crystals containing Rh^{III} ions, colorless HEWL crystals were soaked in buffer solutions containing different concentrations of $RhCl_3$ (0, 1, 5, 10, 30, and 100 mM), 1.8 M NaCl, and 0.1 M NaOAc (pH 4.5) at 20 °C for 2 days (**0-**, **1-**, **5-**, **10-**, **30-**, and **100-Rh·HEWLs**, respectively). The structures of these resulting crystals were refined to a resolution range of 1.40–1.55 Å. Crystallographic data and refinement statistics are listed in Tables S1 and S2 in the Supporting Information. The Rh binding sites were determined by anomalous difference Fourier maps. We solved two individual crystal structures for each set of soaking conditions to confirm the reproducibility of the anomalous difference Fourier maps. The positions of the sodium and chloride ions are distinguished from those of Rh^{III} ions by comparisons with a high resolution Rh^{III}-free HEWL structure.[46] The root-mean-square deviations (rmsds) of the C^{α} atoms of the HEWL crystals soaked with Rh^{III} ions from that of **0-Rh·HEWL** soaked only with buffer are from 0.04 to 0.18, indicating that whole structures of the **Rh·HEWLs** are preserved even during the process of binding of Rh^{III} ions on the pore surfaces of the HEWL crystals.

Rh^{III} binding sites in the pores of 100-Rh·HEWL: Analysis of the crystal structure of **100-Rh·HEWL** indicates that the HEWL monomer has five Rh binding sites located on the surfaces of different pores (Figure 2). Sites A and D are lo-

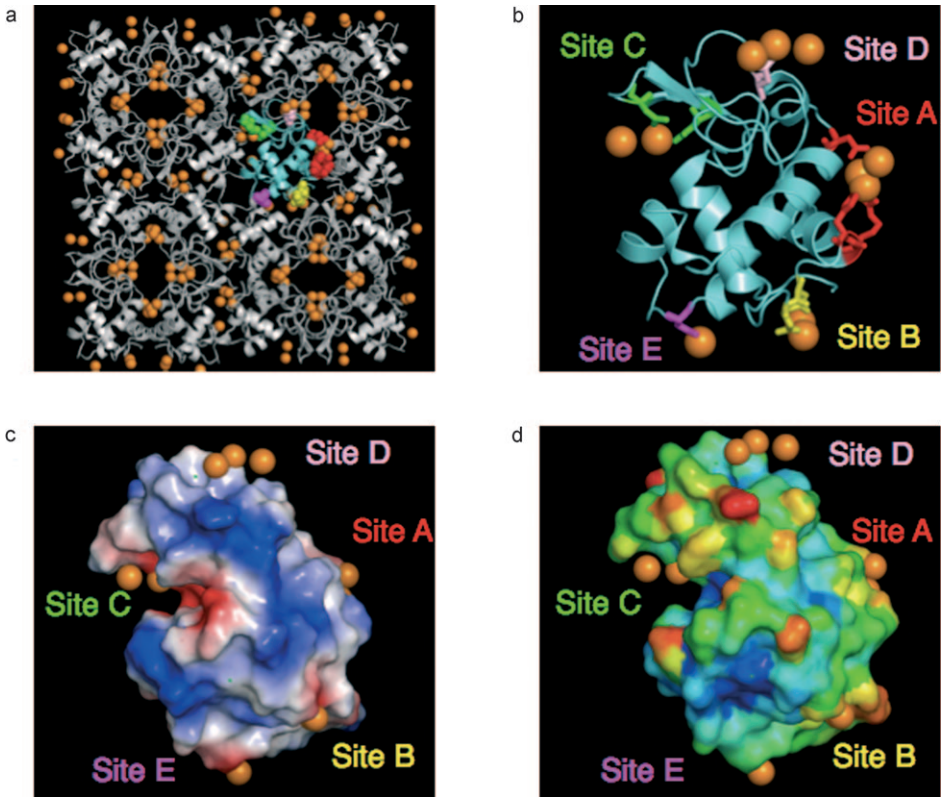

Figure 2. The crystal lattice and molecular structures of **100-Rh·HEWL** (a and b). The monomer is indicated by the cyan structure in a) and b). The molecular surfaces are colored according to c) the electrostatic potential and d) the *B*-factor. Rh atoms are colored with orange. The electrostatic potential for c) is represented by a color spectrum extending from red to blue indicating negative to positive charges for each residue. The surface shown in d) is represented by a color spectrum extending from red to blue for large to small *B*-factor values of each atom. These images were produced by using Pymol.[47]

cated on the largest pore and Sites B, C, and E are found in different narrow pores (Figure 2a). A common factor shared by all of the sites is the presence of negatively charged regions. However, high B-factors of the amino acids do not seem to be essential for metal accumulation (Figure 2c, d). The characteristics of the coordination structures identified at each binding site are described below.

Binding Site A: The anomalous difference Fourier maps of three Rh ions, Rh1, Rh2, and Rh3, are located on the surface of the largest pore of the HEWL crystal (Figure 1 and Figure 3a). This binding site has the ability to trap several types of metal complexes, such as $[Ru(\eta^6\text{-}p\text{-cymene})Cl_2]$, $[Mn(CO)_3]^+$, and $[Pt(NH_3)_2]^{2+}$, by binding to the imidazole moiety of His15.[41–43] The Rh1 atom coordinates to the N^{η} atom of Arg14 and the N^{ε} atom of His15 with bond lengths of 2.12 and 2.35 Å, respectively. These bond lengths are within the usual range of Rh–N bond lengths.[48] The Rh2 atom is bound to an O^{δ} atom of Asp87 (2.01 Å) and a water molecule (O1, 2.20 Å) with typical Rh–O bond lengths.[48] The Rh3 atom is coordinated to three water molecules, but lacks any interactions with the HEWL molecule itself. The bond lengths of Rh1–Rh2, Rh2–Rh3, and Rh1–Rh3 are 3.35, 2.99, and 1.57 Å, respectively. Although O2 serves as a bridging ligand and is located 2.10, 2.48, and 1.87 Å away from Rh1, Rh2, and Rh3, respectively,[49,50] a trinuclear structure is apparently not formed at this site because the 1.57 Å bond length between Rh1–Rh3 is too short to stabilize the trinuclear geometry. This is also supported by the low occupancies of the Rh1 (0.4) and Rh3 (0.6) atoms. A similar observation was reported for ferritin containing Au^{III} ions.[24]

Binding Site B: There have been no previous reports of metal ions binding to this site, which is located on a narrower pore (Figure 3b). Two Rh atoms, Rh4 and Rh5, coordinate with $O^{\delta}1$ (Asp18), O^{δ}-(Asn19), and water molecules. An oxygen atom (O3) serves as a bridging ligand with Rh4–O3 and Rh5–O3 bond lengths of 2.22 and 2.16 Å, respectively.[49] The short length of the Rh4–Rh5 bond (2.76 Å) also suggests the existence of a OH-bridged dinuclear structure.[49]

Binding Site C: It is known that Asn46 and Asp52 can bind metal ions such as Co^{II}, Ni^{II}, Gd^{III}, and Yb^{III} with different coordination geometries.[39,40] Two types of Rh^{III} mononuclear complexes are individually formed at this site (Figure 3c). The electron density at Rh6 indicates that four water molecules are bound to the metal atom. The coordination of water molecules is apparently stabilized by hydrogen bonds with both the side chain and the backbone of Thr47 (Figure 3c).[51] The Rh7 atom is bound to the O^{δ} atoms of Asn46 and Asp52 with bond lengths of 2.00 and 2.19 Å, respectively. The coordination geometry is very similar to that of a previously reported Gd^{III} aqua complex located at the site.[40] There are no oxygen atoms available to form bridged Rh dinuclear centers.

Binding Site D: This binding site, which is located in the largest channel, has not previously been observed to accumulate metal ions.[38–44] We observe that the Rh8 and Rh9 atoms are fixed at this site by coordination to the N^{δ} and O^{δ} atoms of Asn65 at bond lengths of 2.12 and 2.15 Å, respectively. The Rh8–Rh9 distance of 3.03 Å is not sufficient to form a Rh dinuclear complex, although the Rh8–O4 distance of 3.19 Å is too long to allow O4 to form a bridge between Rh8 and Rh9.[49] The Rh10 atom, which only coordi-

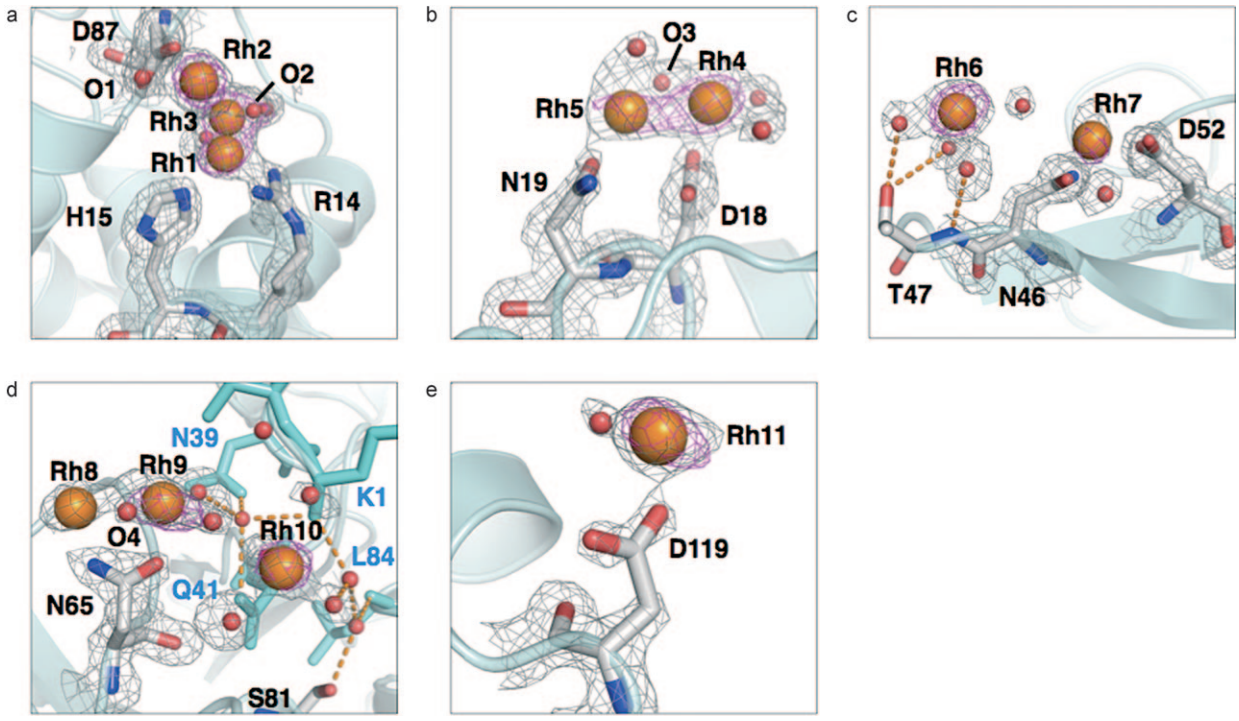

Figure 3. Structures of a) Site A, b) Site B, c) Site C, d) Site D, and e) Site E of **100-Rh·HEWL**. The Rh atom and oxygen of water or OH^- are represented by using spherical models colored with orange and red, respectively. The neighboring HEWL molecule in panel d) is indicated by a cyan-colored tube models. Anomalous difference Fourier maps at 4.0σ indicating the positions of individual Rh atoms are indicated by magenta coloring. The selected $2|F_o|-|F_c|$ electron-density maps at 1.0σ are shown in gray. Hydrogen bonds are indicated with orange dotted lines.

nates to water molecules, is stabilized by a hydrogen-bonding network within the crevice formed by the intermolecular association of two HEWL molecules (Figure 3d).

Binding Site E: This site, which is located within a narrower channel, has been previously reported to have the capability to capture a Gd-HPDO3A complex by hydrogen bond interactions.[38] In the present work, Rh11 is directly bound to the O^δ of D119 and to a water molecule with bond lengths of 1.98 and 2.28 Å, respectively (Figure 3e). No other interactions with Rh11 are observed.

Snapshot analysis of rhodium accumulation: The snapshot analysis of Rh^{III} ion accumulation on the pore surfaces of HEWL crystals was carried out by X-ray crystal structure analysis of the HEWL crystals soaked in buffer solutions containing different amounts of Rh^{III} ions (0, 1, 5, 10, 30, 100 mM, which correspond to the different snapshots in Figure 4) over the course of 2 days. These structures indicate that sequential binding of Rh^{III} ions is associated with conformational changes and rearrangement of hydrogen bonding networks.

Binding Site A: The crystal structures of **0-** and **1·Rh·HEWLs** show that two water molecules (Oa1 and Oa2) are located at the binding site and fixed by two hydrogen bonds with the N^η atom of Arg14 (Figure 4a, a1 and a2). The side chain of Asp87 is fixed by a hydrogen bond with Thr89 (Figure 4a, a1). When HEWL crystals are soaked in buffer containing 5 mM $RhCl_3$, a single anomalous difference Fourier map assignable to a Rh atom appears at that position instead of the original water molecules of **1-Rh·HEWL** (Figure 4a, a3). The Rh1 atom is bound to both the N^η atom of Arg14 and the N^ε atom of His15 with bond lengths of 2.29 and 2.48 Å, respectively. These bond lengths are slightly longer than typical Rh–N bond lengths (Figure 4a, a3).[48] In 10 mM $RhCl_3$ buffer, the two additional anomalous densities of Rh2 and Rh3 are observed close to the Rh1 atom (Figure 4a, a4). As the concentration of $RhCl_3$ increases from 10 to 100 mM, the bond length between Rh2 and O^δ of Asp87 is shortened from 2.94 to 2.01 Å, which is within the range of a typical Rh–O bond length.[48] An accompanying conformational change of the side chain of Asp87 occurs and the hydrogen bond with Thr89 is maintained (Figure 4a, a4–a6).

Binding Site B: At Site B, two Rh^{III} ions are captured and large conformational changes of Asp18 and Asn19 are induced by disruption of a hydrogen-bond network (Figure 4b). In the absence of $RhCl_3$, the side chain of Asp18 is revealed as dual conformer and Asn19 participates in a hydrogen-bond network (Figure 4b, b1). As the $RhCl_3$ concentration increases from 0 to 10 mM, the amide plane (C^β-C^γ-($=O^\delta$)-N^δ) of Asn19 rotates along the C^β–C^α axis and flips to orient the amide O^δ of Asn19 toward Asp18 by shortening the distance between the N^δ atom of Asn19 and the O

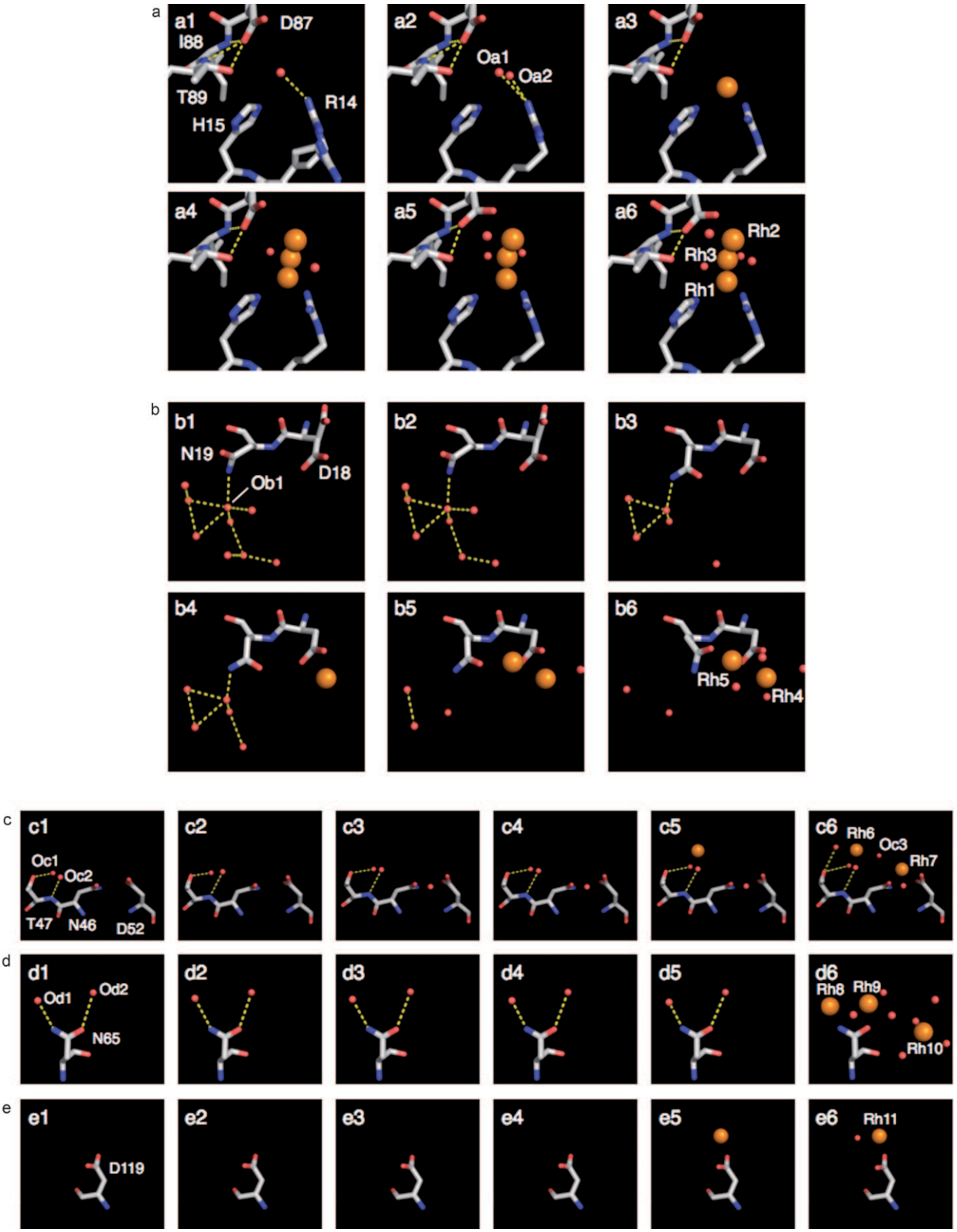

Figure 4. Snapshot analyses of Rh ion binding to a) Site A, b) Site B, c) Site C, d) Site D, and e) Site E. Each structure obtained at a different concentration of $RhCl_3$ is indicated by a-e1, a-e2, a-e3, a-e4, a-e5, and a-e6, representing 0, 1, 5, 10, 30, and 100 mM of $RhCl_3$, respectively, in sodium acetate buffer at pH 4.5. The Rh and O atoms are indicated by orange and red spheres, respectively. The yellow dashed lines indicate hydrogen bonds. The side chains of Asp18 in b1 and b2 are revealed as dual conformers.

atom of a water molecule (Ob1) from 2.73 to 2.45 Å (Figure 4b, b1–b4). The O^{δ} atom of Asp18 is bound to a Rh^{III} ion with side-on geometry in **10-Rh·HEWL** (Figure 4b, b4). The **30-Rh·HEWL** structure shows that additional electron density of a Rh atom (Rh5) occurs between Asp18 and Asn19, and the hydrogen bond of Ob1 and Asp19 is cleaved. In **100-Rh·HEWL**, the distance between the O^{δ} atom of Asn19 and Rh5 is shortened from 2.63 to 2.06 Å in **30-** and **100-Rh·HEWL**, respectively. This appears to be due to the dramatic conformational change of Asn19. Finally, Rh4 and Rh5 form a dinuclear center with a bridged OH ligand (Figure 4b, b6). These results suggest that the cleavage of the hydrogen bond and the conformational change of Asn19 cooperatively contribute to form the dinuclear coordination geometry (Figure 4b).

Binding Site C: The structures of **0–10-Rh·HEWLs** indicate that two water molecules (Oc1 and Oc2) maintain hydrogen-binding interactions with both the side chain and backbone of Thr47 (Figure 4c, c1–c4). These two water molecules can serve as aqua ligands for a Rh^{III} ion in **30-Rh·HEWL** (Figure 4c, c5). When HEWL crystals are soaked in the buffer solution containing 100 mM $RhCl_3$, the other Rh^{III} ion is found to coordinate to Asn46 and Asp52 (Figure 4c, c6). No conformational changes of Asn46, Thr47 and Asp52 were induced during the process of accumulation of these Rh^{III} ions. While there is a water molecule (Oc3) located between Rh6 and Rh7, it is too far from Rh7 (3.39 Å) to serve as a bridging ligand. These results suggest that the each Rh^{III} ion is independently accumulated at this site.

Binding Site D: **0–30-Rh·HEWLs** indicate that N^{δ} and O^{δ} of Asn65 each retain a hydrogen bond with a water molecule (Figure 4d, d1–d5). The two water molecules (Od1 and Od2) were replaced with Rh8 and Rh9 without inducing conformational perturbation of the side chain of Asn65 of **100-Rh·HEWL** (Figure 4d, d6). Moreover, the structure of **100-Rh·HEWL** indicates that an additional mononuclear Rh^{III} aqua complex is independently deposited at the site because no oxygen atoms were found to serve as bridging ligands between Rh9 and Rh10 (Figure 4d, d6).

Binding Site E: The structures of **30-** and **100-Rh·HEWLs** indicate the presence of a Rh^{III} ion binding to D119 (Figure 4e, e4 and e5). The conformational change of the side chain and the hydrogen bond rearrangement were not observed during the binding reaction.

pH Dependence on Rh^{III} binding: To elucidate the pH dependence of Rh^{III} ion binding, **100-Rh·HEWLs** have been prepared by soaking crystals in the buffer solution containing 100 mM $RhCl_3$ at different pH values (4.5, 3.8, and 2.2). The crystal structures at pH 3.8 and 2.2 have been determined at 1.50 and 1.75 Å resolution, respectively (see Table S1 in the Supporting Information and Figure 5). At pH 3.8, the whole structure of **100-Rh·HEWL** indicates the presence of six Rh atoms located the five binding sites observed in **100-Rh·HEWL** at pH 4.5. The conformations of the side chains are similar at pH 3.8 and at pH 4.5 (Figure 5a,b). Rh^{III} aqua complexes at Sites C and D are fixed by hydrogen bonds with the surrounding amino-acid residues (Figure 5b). No Rh atoms are found to coordinate with Asn19, Asn46, Asp52, and Asn65. At pH 2.2, there are four Rh atoms remaining at Sites A, B, C, and D. At Site A, Arg14 adopts two conformers, one of which coordinates to the Rh atom as shown in Figure 5f. The conformation of Asp87 which prevents it from binding its corresponding Rh^{III} ion reverts to that of **0-Rh·HEWL** (Figure 4c and Figure 5f). Although Rh ions are dissociated from Asp52, Asp119, and Asp87, owing to their pK_a values being less than 2.3, Asp18 ($pK_a = 2.3$) conserves coordination with a Rh^{III} ion (Figure 5i).[52,53] At that time, the side chain of Asn19 is in an oppositely-oriented conformation from Asp18 (Figure 5i). At pH 2.2, the Rh^{III} aqua complexes at Sites C and D still remain fixed by hydrogen-bonding interactions with neighboring amino acid residues (Figure 5b, c).

Accumulation mechanism of Rh^{III} ions in the HEWL crystal: Rh^{III} ions can bind to multiple binding sites in the HEWL crystal, as shown in Figure 2. The accumulation process of each Rh^{III} ion at different binding sites is observable by using the HEWL crystals, as the water exchange rate of Rh^{III} is 10^{15} to 10^{13}-fold lower than the water exchange rate of other metal ions, such as Co^{II} and Ni^{II},[30] and because the conversion of mononuclear Rh^{III} aqua complexes into polynuclear Rh^{III} aqua complexes can be easily promoted under the conditions used for crystallization of HEWL (pH 4.5).[50,54] In fact, Rh^{III} dinuclear structures can be found at Sites A, B, and D (Figure 4). Although several structures of HEWL crystals that contain metal ions or metal complexes have been determined, this work represents the first example of using HEWL crystals to elucidate metal accumulation processes. Di- and trivalent metal ions such as Co^{II}, Ni^{II}, Yb^{III}, and Gd^{III} ions are known to ligate to Asp52 and to form hydrogen bonds between their aqua ligands and the neighboring residues at Site C.[39,40] It was concluded that the quantity of Ni^{II} ions and their coordination structures are not affected by the concentration of Ni^{II} ion.[55] Metal complexes, such as $[Mn(CO)_3]^+$, $[Pt(NH_3)_2]^{2+}$, and $[Ru(\eta^6\text{-}p\text{-cymene})Cl_2]$, can be recruited to Site A by coordination with His15 and by hydrophobic interactions with the surrounding residues.[41–43] These metal ions and complexes cannot form polynuclear structures under the conditions used for crystallization. For example, Co^{II} and Ni^{II} ions form polynuclear compounds at high concentrations (> 0.1 M) and pH range (pH 8–11).[30] Therefore, the Rh^{III} ion/HEWL crystal system is appropriate for use as a biomimetic model to elucidate the processes of metal accumulation on protein surfaces.

The crystal structures obtained at pH 4.5 suggest that different hydrogen-bond interactions, as well as coordination of metal ions with amino acid residues, contribute to the promotion of the accumulation process at each binding site by i) regulating the orientation of amino-acid residues for

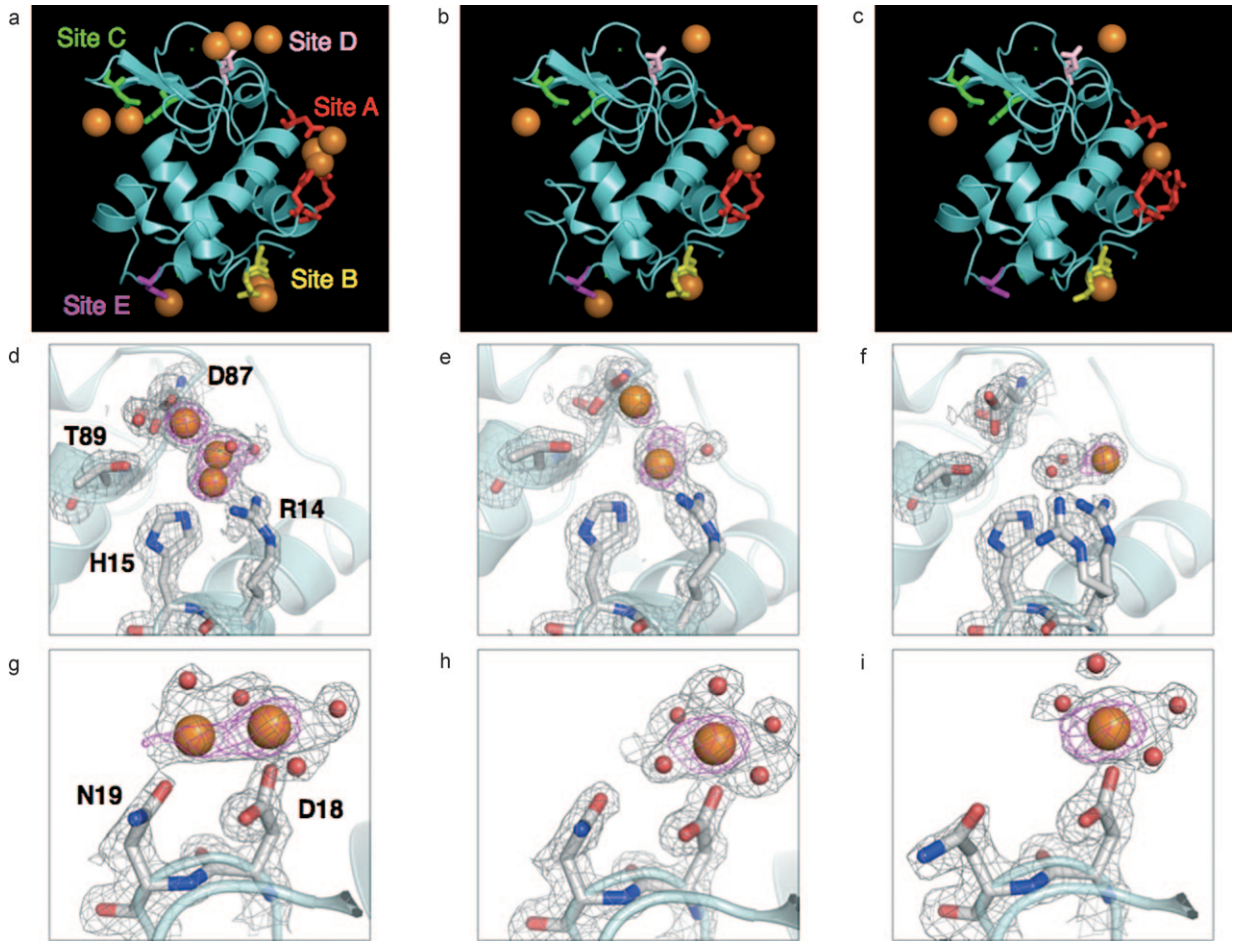

Figure 5. Comparison of crystal structures of **100-Rh·HEWL** prepared at pH 4.5 (a, d, and g), pH 3.8 (b, e, and h), and pH 2.2 (c, f, and i). The Rh atoms are indicated by orange spheres. The O atoms of water molecules or OH^- ions are shown as red spheres. The selected $2|F_o|-|F_c|$ electron density maps at 1.0σ are shown in gray. The anomalous difference Fourier maps at 4.0σ indicate the positions of individual Rh atoms and are indicated by magenta coloring. The side chain of Arg14 in f) is revealed as a dual conformer.

coordination with metal ions (Figure 4a, b), ii) causing water molecules to capture metal ions (Figure 4c), and iii) inducing pre-organization of water molecules at specific amino acid functional groups before the coordination of Rh^{III} ions (Figure 4d). When Rh2 is bound after deposition of Rh1 at Site A, the carboxylate of Asp87 can alter its orientation and bind the Rh2 atom as a result of a strong hydrogen-bond interaction with Thr89. This encourages the formation of stable multinuclear structures at that position (Figure 4a). The conformation of Asn19 is fixed at Site B of **0–10·Rh·HEWLs**, because the side chain is a part of a hydrogen-bond network (Figure 4b). Interestingly, the side chain is taken out of the network by soaking HEWL crystals in buffers with concentrations of $RhCl_3$ greater than 30 mM. The conformation is then dramatically changed to capture Rh5, as observed in **30-** and **100-Rh·HEWLs** (Figure 4b, b5 and b6). The disruption of the hydrogen bond between a water molecule and Asn19 appears to represent a trigger for initiation of coordination of this residue with the Rh5 atom. As shown in Figure 4c, two water molecules are pre-arranged with Thr47 by hydrogen bonds at Site C of **0-Rh·HEWL**. Analysis of the structure of **30-Rh·HEWL** shows that the hydrogen-bonded water molecules are used as two aqua ligands to fix a Rh^{III} ion (Figure 4c, c5). The amide group of Asn65 at Site D forms two hydrogen bonds with two independent water molecules, as observed in **0–30-Rh·HEWLs**. These two water molecules are then replaced by two Rh^{III} ions which form a dinuclear center in **100-Rh·HEWL** (Figure 4d). Therefore, the snapshot analysis suggests that the hydrogen bonds contribute to stabilization of metal coordination structures, as well as multinuclear structures and facilitate the accumulation of metal ions in the binding sites by cooperatively-induced structural changes of the neighboring amino-acid residues.

The pH dependence of **100-Rh·HEWL** structures indicates that the behavior of Rh^{III} aqua complexes interacting with HEWL is different from the behavior of Rh^{III} ions coordinating with amino-acid residues. As the pH is decreased from 4.5 to 2.2, Rh^{III} ions are dissociated from their coordinating amino-acid residues, as shown in Figure 5. In particular, the process of dissociation of Rh^{III} ions from aspartate residues generally tracks the pK_a value of the Asp residues

as determined in solution.[52,53] The Rh^{III} ion bound to Asp52 ($pK_a = 3.4$) is removed at pH 3.8. At pH 2.2, Asp87 ($pK_a = 2.3$) and Asp119 ($pK_a = 3.1$) each release a Rh^{III} ion, whereas Asp18 ($pK_a = 2.3$) remains bound to its Rh^{III} ion. Further investigations will be required to elucidate the stability of the Rh^{III}-ion–Asp18 interaction when the pH is below the p*K*a value of the residue. The aqua complexes at Sites C and D remain at low pH without evidence of significant structural perturbation resulting from the hydrogen bonds of the aqua ligands that interact with the surrounding amino acid residues (Figure 3c, d, and Figure 5b, c). These results imply that the structures of the accumulated metal aqua complexes are stabilized by hydrogen bonds in a wider pH range than metals coordinated by the functional groups of amino-acid residues.

Implications for native metal accumulation and applications thereof: The crystal structures of native metal storage proteins indicate that metal accumulation reactions are promoted according to molecular mechanisms similar to those proposed as a result of our investigations of HEWL crystals that contain Rh^{III} ions. Fbp contains a phosphate anion captured at the iron binding site by hydrogen bonds in the absence of iron atoms.[16] When apo-Fbp crystals are soaked into the precipitant buffer containing $[Fe_2(cit)_2(H_2O)_2]^{2-}$ (cit = citrate), the phosphate anion is replaced by a trinuclear Fe_3O_{13} cluster stabilized by coordination to two conserved Tyr residues and hydrogen bonds with the neighboring residues.[16] This initiation step, triggered by rearrangement of hydrogen bonds, is similar to that of Site B of **Rh·HEWL** (Figure 4b). DpsA has a large cluster of water molecules at the Fe_4O_3 cluster binding site.[15] The water cluster is removed by formation of a Fe_4O_3 cluster there after incubation of apo-Dps crystals into the precipitant solution containing excess $FeCl_2$, as observed at Site D of **Rh·HEWL** (Figure 4d). The crystal structures of ferritins containing different amounts of Pd^{II} ions indicate that Asp and His residues are pre-organized by hydrogen bonds with water molecules at the metal binding site in the apo-form. These Asp and His functional groups can be bound to Pd^{II} ions with cooperative disruption of the hydrogen bonds and alterations of the conformation of coordinated amino acids in a manner similar to that which occurs at Site B of **Rh·HEWL** (Figure 4a).[23] Therefore, it is suggested that these metal clusters in native proteins are formed by accumulation of aqua metal complexes. The reactions are coupled with the rearrangement of hydrogen bonds and conformational changes of amino acid residues, as observed in our model systems.

Metal accumulation processes on protein surfaces have been used in the preparation of various types of inorganic nanomaterials.[4] Genetically modified ferritin, chaperonin, icosahedral virus, tobacco mosaic virus, and bacteriophage M13 virus can serve as templates for selective deposition of metal ions providing nano-particles and wires.[7,11,56,57] Although electrostatic interactions between metal ions and charged residues have been recognized as the most important factors in the design of these proteins for the preparation of inorganic materials,[58–60] the processes of coordination of metal aqua complexes and rearrangement of hydrogen bonds observed in our model systems should be considered as additional key factors for protein-based synthesis of desired inorganic materials. Moreover, we propose that the preparation of inorganic materials by using HEWL in solution is initiated by the mechanism described herein.[35–37]

Conclusion

We have directly observed the process of accumulation of Rh^{III} ions onto internal surfaces of porous hen egg white lysozyme (HEWL) crystals in an effort to clarify initiation steps of the process of accumulation of metals onto protein surfaces. The experimental results produced by using this model system reveal several noteworthy implications for initiation of the process of metal accumulation onto protein surfaces which involve highly cooperative dynamic behavior of amino acids and hydrogen bonds: i) Disruption of hydrogen bonds can induce conformational changes to capture metal ions. ii) Water molecules pre-organized by hydrogen bonds can act as aqua ligands for the stabilization of coordination complexes. iii) Water molecules participating in hydrogen bonds with amino acid residues can be replaced by metal ions to form polynuclear structures involving the amino acid residue. iv) Metal aqua complexes remain bound to amino-acid residues by hydrogen bonds even at low pH. These metal–protein interactions induce inorganic materials prepared in natural biological systems and may also be applicable for the design of new inorganic materials by using protein scaffolds. On the basis of these findings, further efforts to design nanomaterials by using porous HEWL crystals are in progress.

Experimental Section

Materials: Hen egg white lysozyme (HEWL) was purchased from Sigma-Aldrich. Other reagents were purchased from TCI (Wako, Nacalai Tesque), and Sigma–Aldrich and were used without further purification.

Crystallization of HEWL: Tetragonal HEWL crystals were grown at 20 °C by using the hanging drop vapor diffusion method.[46] The reservoir solution contained 0.1 M sodium acetate buffer (pH 4.5) and 0.8 M NaCl, and the drop contained 50 mg mL^{-1} HEWL in acetate buffer (3 μL) and the reservoir solution (3 μL). Tetragonal crystals were obtained in three days.

$RhCl_3$ soaking: Soaking drops (6 μL) contained 0–100 mM $RhCl_3$, 0.1 M NaOAc (pH4.5), 1.8 mol L^{-1} NaCl. Soaking was carried out for 2 days at 20 °C, and crystals gradually turned red-yellow.

X-ray crystallographic analysis: Prior to the data collection, crystals were immersed in a precipitant solution containing 20% (w/w) glycerol and subsequently frozen in liquid nitrogen. X-ray diffraction data were collected at 100 K by using a Rigaku FR-E X-ray generator (wavelength: 1.5418 Å, $Cu_{K\alpha}$) and R-AXIS VII detector at the High-Intensity X-ray Laboratory, Nagoya University. The data were processed with the program DENZO and SCALEPACK.[61] The crystal parameters and data collection data are summarized in Table S1 in the Supporting Information.

Refinement: The structures were solved by molecular replacement with MOLREP by using a lysozyme structure (pdb ID: 193L) as the initial model. Refinement of the protein structure was performed by using REFMAC5[62] in the CCP4 suite. Rebuilding was performed by using COOT[63] based on sigma weighted ($2F_o-F_c$) and (F_o-F_c) electron-density maps. About 5% of the observed data were excluded from the refinements and used to calculate the free R (R_{free}) as a monitor of model bias. The Rh binding sites were determined by anomalous difference Fourier maps. The occupancies of all the rhodium atoms were refined to make the B-factors of the Rh atoms below 45 Å^2.

The positions of the Na and Cl ions were distinguished from those of Rh^{III} ions by comparing with a high resolution Rh^{III}-free HEWL structure.[46] Water molecules were positioned to fit residual (F_o-F_c) density peaks with a lower cut-off of 3σ. Residues Arg125 of **5-Rh·HEWL**, Arg125 of **10-Rh·HEWL**, Gln121 and Arg125 of **30-Rh·HEWL**, Gln121 and Arg125 of **100-Rh·HEWL**, Arg65, Gln121 and Arg125 of **100-Rh·HEWL at pH3.8**, Arg125 of **100-Rh·HEWL at pH2.2** were replaced to Ala because electron density of these residues are missing. The models were subjected to quality analysis during the various refinement stages with omit maps and PROCHECK.[64] The refinement statistics are summarized in Table S2 in the Supporting Information. We have solved two individual crystal structures for each soaking condition to confirm the reproducibility of the anomalous difference Fourier maps. Atomic coordinates are deposited in the Protein Data Bank under accession numbers 3A8Z, 3A90, 3A91, 3A92, 3A93, 3A94, 3A95 and 3A96 for **0-**, **1-**, **5-**, **10-**, **30-**, and **100-Rh·HEWLs, 100-Rh·HEWL at pH 3.8, and 100-Rh·HEWL at pH 2.2**, respectively.

Acknowledgements

This work was supported by a grant from the Global COE Program in Chemistry, Nagoya University (to S.A.), a Grant-in-Aid for Scientific Research (Grant 18655054 to T.U.) from the Ministry of Education, Culture, Sports, Science and Technology, Japan, and PRESTO, JST.

[1] S. Mann, *Biomineralization: Principles and Concepts in Bioinorganic Materials Chemistry, Vol. 5*, Oxford University Press, Oxford, **2001**.
[2] L. Addadi, S. Weiner, *Angew. Chem.* **1992**, *104*, 159; *Angew. Chem. Int. Ed. Engl.* **1992**, *31*, 153.
[3] P. Behrens, E. Baeuerlein in *Handbook of Biomineralization, Vol. 2*, Wiley-VCH, Weinheim, **2007**.
[4] M. Uchida, M. T. Klem, M. Allen, P. Suci, M. Flenniken, E. Gillitzer, Z. Varpness, L. O. Liepold, M. Young, T. Douglas, *Adv. Mater.* **2007**, *19*, 1025.
[5] M. Sarikaya, C. Tamerler, A. K. Y. Jen, K. Schulten, F. Baneyx, *Nat. Mater.* **2003**, *2*, 577.
[6] T. Douglas, M. Young, *Nature* **1998**, *393*, 152.
[7] C. B. Mao, D. J. Solis, B. D. Reiss, S. T. Kottmann, R. Y. Sweeney, A. Hayhurst, G. Georgiou, B. Iverson, A. M. Belcher, *Science* **2004**, *303*, 213.
[8] F. C. Meldrum, V. J. Wade, D. L. Nimmo, B. R. Heywood, S. Mann, *Nature* **1991**, *349*, 684.
[9] W. Shenton, D. Pum, U. B. Sleytr, S. Mann, *Nature* **1997**, *389*, 585.
[10] J. N. Cha, G. D. Stucky, D. E. Morse, T. J. Deming, *Nature* **2000**, *403*, 289.
[11] R. A. McMillan, J. Howard, N. J. Zaluzec, H. K. Kagawa, R. Mogul, Y. F. Li, C. D. Paavola, J. D. Trent, *J. Am. Chem. Soc.* **2005**, *127*, 2800.
[12] M. B. Dickerson, K. H. Sandhage, R. R. Naik, *Chem. Rev.* **2008**, *108*, 4935.
[13] G. F. Xu, N. Yao, I. A. Aksay, J. T. Groves, *J. Am. Chem. Soc.* **1998**, *120*, 11977.
[14] Q. Q. Hoang, F. Sicheri, A. J. Howard, D. S. C. Yang, *Nature* **2003**, *425*, 977.
[15] K. Zeth, S. Offermann, L. O. Essen, D. Oesterhelt, *Proc. Natl. Acad. Sci. USA* **2004**, *101*, 13780.
[16] H. Z. Zhu, D. Alexeev, D. J. B. Hunter, D. J. Campopiano, P. J. Sadler, *Biochem. J.* **2003**, *376*, 35.
[17] Y. H. Pan, K. Sader, J. J. Powell, A. Bleloch, M. Gass, J. Trinick, A. Warley, A. Li, R. Brydson, A. Brown, *J. Struct. Biol.* **2009**, *166*, 22.
[18] J. N. Cha, K. Shimizu, Y. Zhou, S. C. Christiansen, B. F. Chmelka, G. D. Stucky, D. E. Morse, *Proc. Natl. Acad. Sci. USA* **1999**, *96*, 361.
[19] E. M. Pouget, P. H. H. Bomans, J. Goos, P. M. Frederik, G. de With, N. Sommerdijk, *Science* **2009**, *323*, 1455.
[20] B. L. d'Estaintot, S. Paolo, T. Granier, B. Gallois, J. M. Chevalier, G. Precigoux, S. Levi, P. Arosio, *J. Mol. Biol.* **2004**, *340*, 277.
[21] J. Trikha, E. C. Theil, N. M. Allewell, *J. Mol. Biol.* **1995**, *248*, 949.
[22] T. Granier, G. Comberton, B. Gallois, B. L. d'Estaintot, A. Dautant, R. R. Crichton, G. Precigoux, *Proteins Struct. Funct. Bioinf.* **1998**, *31*, 477.
[23] T. Ueno, M. Abe, K. Hirata, S. Abe, M. Suzuki, N. Shimizu, M. Yamamoto, M. Takata, Y. Watanabe, *J. Am. Chem. Soc.* **2009**, *131*, 5094.
[24] M. Suzuki, M. Abe, T. Ueno, S. Abe, T. Goto, Y. Toda, T. Akita, Y. Yamadae, Y. Watanabe, *Chem. Commun.* **2009**, 4871.
[25] S. Abe, K. Hirata, T. Ueno, K. Morino, N. Shimizu, M. Yamamoto, M. Takata, E. Yashima, Y. Watanabe, *J. Am. Chem. Soc.* **2009**, *131*, 6958.
[26] S. Abe, J. Niemeyer, M. Abe, Y. Takezawa, T. Ueno, T. Hikage, G. Erker, Y. Watanabe, *J. Am. Chem. Soc.* **2008**, *130*, 10512.
[27] J. Niemeyer, S. Abe, T. Hikage, T. Ueno, G. Erker, Y. Watanabe, *Chem. Commun.* **2008**, 6519.
[28] T. Ueno, M. Suzuki, T. Goto, T. Matsumoto, K. Nagayama, Y. Watanabe, *Angew. Chem.* **2004**, *116*, 2581; *Angew. Chem. Int. Ed.* **2004**, *43*, 2527.
[29] D. Alexeev, H. Z. Zhu, M. L. Guo, W. Q. Zhong, D. J. B. Hunter, W. P. Yang, D. J. Campopiano, P. J. Sadler, *Nat. Struct. Biol.* **2003**, *10*, 297.
[30] D. T. Richens, *The Chemistry of Aqua Ions*, Wiley, New York, **1997**.
[31] A. L. Margolin, M. A. Navia, *Angew. Chem.* **2001**, *113*, 2262; *Angew. Chem. Int. Ed.* **2001**, *40*, 2204.
[32] L. Z. Vilenchik, J. P. Griffith, N. St Clair, M. A. Navia, A. L. Margolin, *J. Am. Chem. Soc.* **1998**, *120*, 4290.
[33] A. Cvetkovic, C. Picioreanu, A. J. J. Straathof, R. Krishna, L. A. M. van der Wielent, *J. Am. Chem. Soc.* **2005**, *127*, 875.
[34] Z. Q. Hu, J. W. Jiang, *Langmuir* **2008**, *24*, 4215.
[35] F. Gao, Q. Y. Lu, S. Komarneni, *Chem. Commun.* **2005**, 531.
[36] H. R. Luckarift, M. B. Dickerson, K. H. Sandhage, J. C. Spain, *Small* **2006**, *2*, 640.
[37] A. E. Voinescu, D. Touraud, A. Lecker, A. Pfitzner, W. Kunz, B. W. Ninham, *Langmuir* **2007**, *23*, 12269.
[38] E. Girard, L. Chantalat, J. Vicat, R. Kahn, *Acta Crystallogr. Sect. A* **2002**, *58*, c83.
[39] S. J. Li, *Biopolymers* **2006**, *81*, 74.
[40] R. A. P. Nagem, Z. Dauter, I. Polikarpov, *Acta Crystallogr. Sect. A* **2001**, *57*, 996.
[41] A. Casini, G. Mastrobuoni, C. Temperini, C. Gabbiani, S. Francese, G. Moneti, C. T. Supuran, A. Scozzafava, L. Messori, *Chem. Commun.* **2007**, 156.
[42] I. W. McNae, K. Fishburne, A. Habtemariam, T. M. Hunter, M. Melchart, F. Y. Wang, M. D. Walkinshaw, P. J. Sadler, *Chem. Commun.* **2004**, 1786.
[43] M. Razavet, V. Artero, C. Cavazza, Y. Oudart, C. Lebrun, J. C. Fontecilla-Camps, M. Fontecave, *Chem. Commun.* **2007**, 2805.
[44] T. M. Hunter, I. W. McNae, X. Y. Liang, J. Bella, S. Parsons, M. D. Walkinshaw, P. J. Sadler, *Proc. Natl. Acad. Sci. USA* **2005**, *102*, 2288.
[45] L. Spiccia, *Inorg. Chim. Acta* **2004**, *357*, 2799.
[46] M. Cianci, J. R. Helliwell, A. Suzuki, *Acta Crystallogr. Sect. A* **2008**, *64*, 1196.
[47] pymol: http://pymol.org/.
[48] U. Rychlewska, M. I. Djuran, M. M. Vasojevic, D. D. Radanovic, V. M. Ristanovic, D. J. Radanovic, *Inorg. Chim. Acta* **2002**, *328*, 218.
[49] R. Cervini, G. D. Fallon, L. Spiccia, *Inorg. Chem.* **1991**, *30*, 831.

[50] L. Spiccia, J. M. Aramini, S. J. Crimp, A. Drljaca, E. T. Lawrenz, V. Tedesco, H. J. Vogel, *J. Chem. Soc. Dalton Trans.* **1997**, 4603.
[51] L. N. Kuleshova, P. M. Zorkii, *Acta Crystallogr. Sect. A* **1981**, *37*, 1363.
[52] Y. Abe, T. Ueda, H. Iwashita, Y. Hashimoto, H. Motoshima, Y. Tanaka, T. Imoto, *J. Biochem.* **1995**, *118*, 946.
[53] J. Antosiewicz, J. A. McCammon, M. K. Gilson, *J. Mol. Biol.* **1994**, *238*, 415.
[54] J. S. Forrester, G. H. Ayres, *J. Phys. Chem.* **1959**, *63*, 1979.
[55] S. H. Li, T. Matsuura, H. Tanaka, A. Nakagawa, T. Tsukihara, M. Ataka, *J. Cryst. Growth* **2005**, *276*, 222.
[56] T. Douglas, E. Strable, D. Willits, A. Aitouchen, M. Libera, M. Young, *Adv. Mater.* **2002**, *14*, 415.
[57] E. Dujardin, C. Peet, G. Stubbs, J. N. Culver, S. Mann, *Nano Lett.* **2003**, *3*, 413.
[58] M. Knez, M. Sumser, A. M. Bittner, C. Wege, H. Jeske, T. P. Martin, K. Kern, *Adv. Funct. Mater.* **2004**, *14*, 116.
[59] W. Shenton, T. Douglas, M. Young, G. Stubbs, S. Mann, *Adv. Mater.* **1999**, *11*, 253.
[60] K. Iwahori, K. Yoshizawa, M. Muraoka, I. Yamashita, *Inorg. Chem.* **2005**, *44*, 6393.
[61] Z. Otwinowski, W. Minor, *Methods Enzymol.* **1997**, *276*, 307.
[62] G. N. Murshudov, A. A. Vagin, E. J. Dodson, *Acta Crystallogr. Sect. A* **1997**, *53*, 240.
[63] P. Emsley, K. Cowtan, *Acta Crystallogr. Sect. A* **2004**, *60*, 2126.
[64] R. A. Laskowski, M. W. Macarthur, D. S. Moss, J. M. Thornton, *J. Appl. Crystallogr.* **1993**, *26*, 283.

Received: November 30, 2009
Published online: February 9, 2010

